A new coupled fluid-structure modelling methodology for running ductile fracture

H. O. Nordhagen[1], S. Kragset[2], T. Berstad[1], A. Morin[3], C. Dørum[1], S. T. Munkejord[2]

[1] SINTEF Materials and Chemistry, P.O. Box 7460, NO-7465 Trondheim, Norway

[2] SINTEF Energy Research, P.O. Box 4761 Sluppen, NO-7465 Trondheim, Norway

[3] Norwegian University of Science and Technology (NTNU), Dept. of Energy and Process Engineering, NO-7491 Trondheim, Norway

Corresponding author: cato.dorum@sintef.no

Abstract

A coupled fluid-structure modelling methodology for running ductile fracture in pressurized pipelines has been developed. The pipe material and fracture propagation have been modelled using the finite-element method with a ductile fracture criterion. The finite-volume method has been employed to simulate the fluid flow inside the pipe, and the resulting pressure profile was applied as a load in the finite-element model. Choked-flow theory was used for calculating the flow through the pipe crack. A

comparison to full-scale tests of running ductile fracture in steel pipelines pressurized with hydrogen and with methane has been done, and very promising results have been obtained.

1   Introduction

The world energy use is continuously increasing. Despite the advances in renewable energy, fossil fuel such as oil, coal and gas will provide the major part of the energy many years ahead. As the large reserves of gas typically are far from the market, there is a need to enable safe and cost-efficient gas transportation. Further, it is foreseen that large amounts of CO_2 will be transported as carbon capture and storage (CCS) is deployed [1]. Some of the main challenges in high pressure gas pipeline transport are related to pipeline integrity and fracture control. They comprise constructing suitable modelling tools, obtaining experimental data, and formulating new specifications and requirements for the construction of the pipeline. Due to accidental failure (e.g. through third party impacts or corrosion) or planned maintenance, the pipe can be depressurized. During the depressurization, the escaping gas will cool the pipe. If the temperature becomes low enough, the pipe material may become brittle, causing brittle rupture and severe damage to the pipeline. Long running cracks in high pressure gas pipelines may lead to significant economical losses, and must be avoided. At the same time, the high price of steel requires cost-effective solutions regarding the design of the pipeline.

Although avoidance of brittle fracture is the first step in fracture propagation control, it is assumed that this problem can be solved through e.g. using steel with a very low ductile brittle transition temperature. In this paper the focus is on running ductile fracture (RDF), and on a new method that can

be used to form pipeline design criteria (e.g. minimum thickness or fracture resistance demands) that ensure arrest of RDF within an acceptable number of pipe lengths.

Running ductile fracture is commonly assessed using semi-empirically-based models originating from work done at the Battelle memorial institute in the 1970s [2]. These models assume the fluid and the structure (fracture resistance) to be uncoupled processes. Fracture velocity is empirically correlated to the Charpy energy. As long as the fracture velocity is smaller than the decompression wave velocity, crack arrest is ensured. A variant of this model, known as the Japanese HLP approach [3], can in addition be used to predict the final crack length of a RDF.

Existing methods have several drawbacks. For example, they require cumbersome re-calibration when changing the pressurised fluid inside the pipe, or when new material qualities are introduced. These approaches were developed for pipeline material qualities used 30-40 years ago for transport of natural gas, and worked well in those cases. Due the economical benefits of transporting gas at higher pressures and volumes, the trend seen today is to use pipelines with higher strength and toughness, as well as lower pipe wall thicknesses. The high toughness of these steels causes the relationship between the fracture energy (e.g. Charpy) and the fracture velocity to be uncertain [4]. There are strong indications that the empirical basis developed earlier (Battelle and HLP) does not apply for these new conditions (e.g. [4, 5]) In the case of CO_2-transport, there is a lack of knowledge on how CO_2 will influence on the running ductile fracture problem – both with regard to the depressurization wave speed as well as to the heat exchange aspects. One approach is to perform full scale pipe rupture tests, where the required pipe strength is derived from the toughness of the pipe section in which the propagating crack arrests. Such tests are very expensive and time consuming. Thus, they do not allow for thorough parametric studies.

Running ductile fracture in gas transmission pipelines consists of three interacting events. These are large scale elasto-plastic dynamic deformation of the pipe walls, three-dimensional unsteady gas dynamics, and an inelastic crack extension process [1-11]. Due to this very complex interaction process, only a few numerical models for prediction of running ductile fracture have been developed.

O'Donoghue et al. [6, 7] developed a coupled computational model for simulation of ductile fracture, coupling the structural dynamics from an explicit finite element (FE) code with the fluid flow behaviour calculated by a finite difference program. Later works [8-10] has extended the framework to include crack arrestors, the behaviour of high-strength and high-toughness steel pipeline materials, as well as modelling of rich gas (heavy hydrocarbon natural gas) through a three stage linear decompression model. An alternative approach for modelling fracture propagation was presented by Greenshields et al. [11]. Their model uses a unified platform based on finite volume (FV) discretization for both the structure and fluid analysis, and was developed for brittle fracture in plastic pipes.

There exist numerous approaches to calculating the behaviour of the phenomenon of escaping gas through a crack or nozzle [12-16], but few of these models takes on the difficult task of coupling the structural failure with the fluid behaviour. In a work by Rabczuk et al. [16], a meshfree method for treating coupled fluid-structure interaction of fracturing structures under impulsive loads were described.

The work in this paper presents a new approach for the evaluation of fracture propagation in gas pipelines using a numerical, coupled fluid-structure methodology and a local fracture criterion. The aim is to replace today's empirical basis and to provide an alternative to expensive full scale testing, allowing for sensitivity studies to be performed. The pipe has been modelled in the explicit finite-element (FE) code LS-DYNA [17] using shell elements. The fluid flow inside the pipe has been modelled using a one-dimensional (1D) finite-volume method. Choked-flow theory is used to model the gas flowing out of the

pipe in the region where there is a crack opening. Preliminary results using the approach presented in this paper can be found in [18]. It should be noted that LS-DYNA has the opportunity to run fluid-structure simulations using ALE-formulations (Arbitrary Lagrangian-Eulerian)or SPH(Smoothed Particle Hydrodynamics). However, this would require a relatively large number of ALE-elements or SPH-particles and would therefore be much more CPU-expensive. Furthermore, the long-term ambition with the present work is to develop a methodology that can handle multi-phase flow and phase transformation (relevant for CO_2-transport). Thus, the approach using the 1D finite-volume method was chosen due to numerical efficiency and robustness.

In the simulations, the crack path is modelled as a predefined axially straight "seam" where the elements are allowed to fail. To trigger the RDF, the elements corresponding to an initial crack in full scale experiments are removed. For validation of the methodology, the results from the numerical simulations are compared with experimental data from full-scale testing of X65 steel pipelines containing either high-pressure hydrogen or methane gas at two different initial pressures. See reference [19] for a further description of the full scale experiments.

This work is one step towards the objective of developing a coupled (fluid-structure) fracture assessment model to enable safe and cost-effective design and operation of high-pressure gas pipelines by improving the fundamental understanding of the interaction between the material mechanical and fluid dynamical behaviour.

2   Modelling of the pipeline material

The investigated pipeline structure is API 5L-X65mod ERW steel pipes from Nippon steel, with an outer diameter of 267 mm and wall thickness of 6 mm. The pipe thickness and diameter variation is ±0.07mm and ±2 mm, respectively, between the different pipeline segments used in the full scale experiments.

The chemical composition of the pipeline material is provided in Table 1. After the burst tests had been carried out [19], specimens for material characterization were extracted from parts of the pipes that had not been exposed to permanent deformation during the test.

It is well known that most steel pipeline materials have a certain degree of anisotropic plastic behavior, arising mainly from texturing during the plate rolling process [20, 21]. The pipe forming process also introduces additional anisotropy through pre-straining mainly in the circumferential pipe direction. For simplicity, it has in this work been assumed an isotropic yield criterion (von-Mises). It should be mentioned that the investigated pipe material has Lankford coefficients between 0.6 and 0.8. Upon uniaxial loading, this plastic anisotropy signifies a preferential plastic contraction in the thickness direction. This anisotropy has not been accounted for in the simulations.

A non-linear isotropic work-hardening rule is used. The work-hardening of pipeline steels is known to be affected by both strain rate and temperature. As RDF involves large strain rates (> 100 s^{-1}), strain-rate dependency in the work-hardening rule has been used. The temperature dependency of the material behavior has been neglected. For the plastic strain increments an associated flow rule has been used.

Fracture is modeled by the Cockcroft-Latham ductile fracture criterion [22], and crack propagation is modeled through element erosion. An element is removed when the first integration point in an element has reached the fracture criterion. In the following, the chosen material modeling method will be presented.

2.1 The isotropic visco-plastic constitutive equations

The yield function, f , which defines the elastic domain in stress space, is expressed in the form

$$f\left(\boldsymbol{\sigma},\varepsilon_e\right)=\sigma_e\left(\boldsymbol{\sigma}\right)-\left(\sigma_0+R\left(\varepsilon_e,\dot{\varepsilon}_e\right)\right) \tag{1}$$

where $\boldsymbol{\sigma}$ is the stress tensor, σ_e is the von Mises equivalent stress, ε_e is the corresponding equivalent plastic strain, and σ_0 is the yield stress in the reference direction. The isotropic strain rate dependent work-hardening rule is defined as:

$$
R = \begin{cases}
\left[\sigma_0 + \sum_{i=1}^{2} Q_i (1 - \exp(-C_i \varepsilon_e)) \right] \left[1 + \dfrac{\dot{\varepsilon}_e}{\dot{\varepsilon}_0} \right]^c & , \varepsilon_e \le \varepsilon_c \\[4mm]
\left[S_0 + K(\varepsilon_e)^n \right] \left[1 + \dfrac{\dot{\varepsilon}_e}{\dot{\varepsilon}_0} \right]^c & , \varepsilon_e > \varepsilon_c
\end{cases}
\tag{2}
$$

where Q_i and C_i are the quasi-static hardening parameters, $\dot{\varepsilon}_e$ is the effective plastic strain rate and ε_c is the effective plastic strain at onset of necking (maximum applied force in a uniaxial test). The parameters $\dot{\varepsilon}_0$ and c characterize the strain rate dependency of the hardening curve. After the onset of necking ($\varepsilon_e > \varepsilon_c$) in a uniaxial test, an imposed hydrostatic tension will form in the neck, and the uniaxial stress state must be corrected. This correction is done using FE analysis, where S_{100} (true stress at 100% effective plastic strain) is adjusted such that the experimental and simulated engineering stress-strain curve match. The parameters K and n are automatically adjusted to ensure C^1 when $\varepsilon_e = \varepsilon_c$. Prediction of necking is ensured through the calibration of Q_i and C_i.

The work-hardening parameters in equation (2) were calibrated from tensile tests of smooth axisymmetric specimens oriented in the circumferential direction (reference direction) of the pipe. Quasi-static tests were carried out at room temperature at an average strain rate of 10^{-3} s^{-1}. Three parallel tests were done and the scatter between the tests was found to be negligible. The force and the diameter at minimum cross-section of the specimen were continuously measured until fracture. This was done using a purpose-built measuring rig where two perpendicular lasers accurately measured the specimen diameters. To ensure that the diameter readings always were measured at the minimum cross-section, the lasers were installed on a mobile frame. Based on the diameter and force

measurements the true stress was calculated. For a more detailed description of the calculation of the true stress and effective plastic strain, see e.g. Børvik et al. [23].

The parameters identified for the quasi-static work-hardening law are given in Table 2. Figure 2 shows the experimental and simulation results of the stress-strain curves of the uniaxial test in reference direction at quasi-static conditions.

The parameters $\dot{\varepsilon}_0$ and c representing the strain-rate dependent flow stress law was calibrated through uniaxial tensile tests at strain rates in the range 10^{-4}–10^3 s^{-1}. For strain rates larger than 10^2 s^{-1} a split-Hopkinson tension bar (SHTB) was used (similar to the one described in [24]). By plotting the true stress at a given plastic strain as a function of the strain rate, $\dot{\varepsilon}_0$ and c (in Equation 2) was adjusted to obtain a fit. In Figure 3, the experimental flow stress at different strain rates – as well as the strain-rate dependent part of Eq. 2 using $\dot{\varepsilon}_0$ =1.5x10^{-2} s^{-1} and c =1.1x10^{-2} have been plotted. Note that the strain rate parameters were derived from specimens oriented perpendicular to the reference direction. However, the authors do not expect to observe any anisotropy in the strain rate dependency of the investigated steel materials.

2.2 The fracture model

From the perspective of material modeling, the greatest obstacle to simulate RDF is the lack of fundamental understanding of the processes governing dynamic ductile fracture (see e.g. [25, 26]) and how to characterize the dynamic fracture resistance of the material. A RDF in a pressurized pipeline runs axially along the pipe at velocities reaching 100-300 m/s [1-10, 27, 28]. The fracture surfaces are oriented approximately 45 degrees through the thickness of the pipe – often termed as slant fracture. The physical mechanisms responsible for the slant fracture formation is debated [25, 26] and can be considered unknown. It is likely that a through-thickness localization of plastic strains (as often seen in

plane-strain testing [29]), followed by a combination of void sheeting and adiabatic heating due to plastic deformation, causes a plastic instability that finally leads to fracture. In this work, a simplified approach to describe fracture is adopted. The influence of damage evolution (e.g. void growth) on the material behavior is neglected. This implies that there is no material softening before initiation of fracture. Crack propagation is described by element erosion when the ductile fracture criterion proposed by Cockcroft and Latham is fulfilled within the element (only one integration point):

$$W = \int \max\left(\sigma_1, 0\right) d\varepsilon_e \leq W_c \quad .$$ (3)

Herein, σ_1 is the maximum principal stress, and W_c is a material parameter that should be determined from a suitable experiment. This criterion has the dimension of work per unit volume, and implies that fracture is a function of the tensile (principal) stress σ_1 and equivalent plastic strain ε_e,. Note that the used failure criterion describes a marked effect of the stress state on the ductility of the material, and that fracture will never occur for stress paths in which all principal stresses are negative.

In this work, W_c has been calibrated from uniaxial tests using axisymmetric smooth bars (SHTB specimen) at quasi-static loading conditions (strain rate equal to $10^{-3}\,\mathrm{s}^{-1}$). The value of W_c was found by integrating the true stress-plastic strain curve up to the point of failure. Results from calibration of the CL criterion calibration gave W_c = 1200 (±80) MPa.

3   The fluid model

Since the fluid pressure is the driving force of the propagating crack, an accurate description of the pressure profile in the vicinity of the crack tip is crucial for the performance of the coupled model. On the other hand, the pressure profile is determined by the position and size of the crack opening, thus there is a two-way coupling between the fluid and structure models. Section 3.1 describes the fluid

model and how the flow through the crack is accounted for by source terms representing the leakage of the fluid through the opening. The numerical method is presented in section 3.2.

3.1 Governing equations

The one-dimensional flow of a single-phase fluid through a pipeline can be modelled at time t and position x by the one-dimensional Euler equations,

$$
\begin{aligned}
\frac{\partial \rho}{\partial t} + \frac{\partial(\rho u)}{\partial x} &= 0, \\
\frac{\partial(\rho u)}{\partial t} + \frac{\partial(\rho u^2)}{\partial x} + \frac{\partial p}{\partial x} &= 0, \\
\frac{\partial E}{\partial t} + \frac{\partial\left[(E+p)u\right]}{\partial x} &= 0,
\end{aligned}
\tag{4}
$$

where ρ, p and u are the density, the pressure and the x-directed velocity, respectively. The total specific energy of the fluid can be written $E = \rho(e + u^2/2)$, where e is the specific internal energy. By adding source terms to the right-hand side of the equations, e.g. wall friction can be included. In this study, these equations are used to model the pipeline flow subject to a running ductile fracture. Source terms account for the leakage of fluid through the crack.

Consider temporarily the tree-dimensional version of the Euler equations (4) rewritten in their integral form,

$$
\begin{aligned}
\frac{\partial}{\partial t}\int_V \rho\,dV + \int_S \rho\mathbf{u}\cdot\mathbf{n}\,dS &= 0, \\
\frac{\partial}{\partial t}\int_V \rho u\,dV + \int_S \rho\mathbf{u}(\mathbf{u}\cdot\mathbf{n})\,dS + \int_S p\mathbf{n}\,dS &= 0, \\
\frac{\partial}{\partial t}\int_V E\,dV + \int_S (E+p)\mathbf{u}\cdot\mathbf{n}\,dS &= 0.
\end{aligned}
\tag{5}
$$

Here, $\mathbf{n}$ is the unit vector normal to the surface S enclosing the volume V. When the integrals are evaluated sectionwise in the infinitesimal volumes $V = A\,dx$ (see Figure 1), the sections behind the crack

tip will contain both the longitudinal flow and the *y*-directed leakage though the crack. The equations can then be recast back into the 1D differential form,

$$\frac{\partial \rho}{\partial t} + \frac{\partial(\rho u)}{\partial x} = -\zeta_e,$$

$$\frac{\partial(\rho u)}{\partial t} + \frac{\partial(\rho u^2)}{\partial x} + \frac{\partial p}{\partial x} = -u\zeta_e, \qquad (6)$$

$$\frac{\partial E}{\partial t} + \frac{\partial[(E+p)u]}{\partial x} = -(E_e + p_e)\frac{1}{\rho_e}\zeta_e,$$

where the additional source term

$$\zeta_e = \rho_e u_e \frac{2r_e}{A} \qquad (7)$$

now represents the mass loss due to the escape of the fluid through the crack of width $2r_e$, which generally is a function of the position *x.*

Ahead of the crack tip, it is reasonable to assume the flow to be one-dimensional, but this assumption does not hold behind the crack tip. However, the added source terms can effectively account for the *y*-directed escape flow due to the leakage of the fluid through the crack opening. As the opening widens, the one-dimensional character of the fluid flow will naturally degenerate, but this is believed to be less important with respect to the crack propagation.

With a suitable equation of state (EOS), the escape quantities, denoted with subscript *e*, can be expressed as functions of the state of the fluid within the pipe, as well as of the crack opening width $2r_e(x)$ and the surrounding pressure. For single-phase flow of gases well above their critical point, the ideal gas EOS

$$p = (\gamma - 1)e\rho, \qquad (8)$$

where $\gamma = c_p/c_v$ is the ratio of the specific heats, works sufficiently well. Initially, when the inside to outside pressure ratio is larger than or equal to the choked flow criterion $[(\gamma + 1)/2]^{\gamma/(\gamma - 1)}$, the flow velocity will attain but not exceed the speed of sound. The flow is then said to be choked or critical. If one assumes that the escape flow is an isentropic process, the following expressions result:

$$\rho_e = \rho \left(\frac{2}{\gamma+1} \right)^{1/(\gamma-1)}, \qquad (9)$$

$$u_e = a_e = a \sqrt{\frac{2}{\gamma+1}}, \qquad (10)$$

where a is the speed of sound in the fluid. When the inside to outside pressure ratio falls below the choked flow criterion, it is still possible to derive the corresponding expressions,

$$\rho_e = \left(\frac{p_a}{p} \right)^{1/\gamma} \rho, \qquad (11)$$

$$u_e = a \left\{ \frac{2}{\gamma-1} \left[1 - \left(\frac{p_a}{p} \right)^{(\gamma-1)/\gamma} \right] \right\}^{1/2}. \qquad (12)$$

For an on-shore pipeline, the surrounding pressure p_a usually corresponds to the atmospheric pressure, and that has been assumed in the following calculations. The above results can easily be adapted to include the slightly more general "stiffened gas" equation of state. It is an extension of the ideal gas EOS, better suited to liquids. A pressure offset p_∞ is included to allow a non-zero density at zero pressure. p and p_a are simply replaced by $(p + p_\infty)$ and $(p_a + p_\infty)$, respectively, and the ratio $(p + p_\infty) / (p_a + p_\infty)$ is used when assessing the choked flow criterion.

3.2 Numerical solution

The governing equations (6) are discretized using the finite-volume method. They are then solved numerically employing the multi-stage centred (MUSTA) scheme by Toro and co-workers [30,31]. The MUSTA scheme has been investigated and found to be robust and accurate for different two-phase flow models, including drift-flux [32,33] and two-fluid [34] models.

The equation system (6) can be cast in the following form

$$\frac{\partial \mathbf{q}}{\partial t} + \frac{\partial \mathbf{f}(\mathbf{q})}{\partial x} = \mathbf{s}(\mathbf{q}) \tag{13}$$

where $\mathbf{q} = [\rho, \rho u, E]^{\mathrm{T}}$ is the vector of conserved variables, $\mathbf{f} = [\rho u, \rho u^2 + p, (E+p)u]^{\mathrm{T}}$ is the flux vector and $\mathbf{s}$ is the source-term vector. Employing the finite-volume method, we obtain the discretized system

$$\mathbf{q}_j^{m+1} = \mathbf{q}_j^m - \frac{\Delta t}{\Delta x}\left(\mathbf{f}_{j+1/2}^m - \mathbf{f}_{j-1/2}^m\right) + \mathbf{s}_j^m \tag{14}$$

where $\mathbf{q}_j^m$ denotes the numerical approximation to the cell average of the vector of unknowns $\mathbf{q}(x_j, t_m)$ in control volume j at time step m. In the MUSTA scheme, the numerical flux at the cell interface $j+1/2$ is a function of the cell averages on each side

$$\mathbf{f}_{j+1/2} = \mathbf{f}^{\mathrm{MUSTA}}\left(\mathbf{q}_j, \mathbf{q}_{j+1}\right). \tag{15}$$

Further details can be found in References [30,32].

4 Numerical modelling of running ductile fracture

This section briefly explains how the fluid-dynamic model is coupled to the structural mechanics model. Further, information is provided regarding the burst tests employed to validate the coupled model.

4.1   The fluid-structure coupling scheme

A numerical methodology for simulation of crack propagation and arrest through a coupling of fluid and structural/fracture mechanics has been established in this work. The pipe has been modelled in the explicit finite-element (FE) code LS-DYNA. To avoid dynamic effects of the generation of the initial pressure, as well as speeding up the initial phase of the simulations, an implicit scheme is used to set the initial pressure in the pipe. Upon initiation of the fracture, a switch from the implicit to an explicit scheme is done. The fluid flow inside the pipe has been modelled using a one-dimensional finite-volume method, where in any cross-section the pressure is taken to be uniform. The coupling between LS-DYNA and the fluid code is done through a user-defined loading subroutine in LS-DYNA where the fluid code is called. At each time step, the fluid code calculates an updated pressure profile for the longitudinal direction of the pipe. This pressure is applied as a load (boundary condition) in the structural FE code. Dynamic fracture is initiated by removing a number of elements corresponding to the length of the directed explosive charge in the full-scale tests, see below.

4.2   Burst tests

The proposed numerical methodology for evaluation of RDF in steel pipelines has been validated by comparing numerical predictions of fluid pressure and crack propagation length with experimental measurements obtained from full-scale testing [19]: A series of four full scale burst tests have been conducted on API 5L-X65mod. ERW pipes with outer diameter of 267 mm and wall thickness of 6 mm. Two tests were performed with hydrogen gas with initial pressures equal to 121 and 151 bar, and two tests were performed with methane gas with initial pressures equal to 122 and 152 bar. This corresponds to hoop stresses of about 0.60 and 0.75 SMYS, respectively. An initial crack length of 30 cm, ensured to be well above failure conditions, was used to initiate the experiments. The initial crack was generated using a directed explosive. An 11.5 meter pipe segment was used for the methane tests. Due

to the almost three times higher speed of sound in hydrogen, the hydrogen gas tests were performed on longer pipes (34.5m). This was done to avoid that the reflecting gas-decompression wave could reach the crack tip before arrest. Illustrations of the full scale experimental test set-ups are shown in Figure 5. No backfill was used on the section of the pipe where the crack propagated. Pressure transducers were placed in a three o'clock position at an axial distance of 1 m and 3 m from the initial crack for the methane gas tests, and 1 m and 4 m for the hydrogen gas tests. Timing wires were used to monitor the crack tip position during the full scale experiments. For more details about the full scale testing, it is referred to the publication by Aihara et al. [19].

The data that are used to validate the proposed fluid-structure coupled model consists of the following list of observations from the full scale experiments:

- Pressure measurements from sensors at 1 and 3 (4) meters

- Crack position and crack velocity measurements from the timing wire data

- Final shape of the fractured pipe

4.3   The FE mesh

As discussed earlier, a neck travelling in front of an RDF – with a correspondingly large area of plastic thinning of the pipe material – will account for most of the work done by the escaping gas. Although the specific fracture energy is orders of magnitude less than the total work, the fracture criterion controls the extension and amount of thinning of the pipe during the RDF – and therefore also the fracture velocity. It is well known that the element type and size play an important role in numerical simulation of plastic instability and fracture [35, 36, 37]. In this work, the default shell element in LS-DYNA is used (Belytschko-Tsay with one in-plane integration point). As noted in a previous work by Dørum et al. [35]; when modelling strain localization with shell elements, it is important to keep in mind the limitation of the element formulation, namely that the out-of-plane normal stress is assumed to be zero. In shell

simulations, the stabilizing tri-axial stress state arising in necking regions is excluded, whereby it is expected that strain localization occurs earlier than in simulations with solid elements. The width of the localized neck that develops in thin-walled materials is typically of the order of the thickness. For shell elements the width of the local neck is independent of the thickness and typically equal to the width of the elements. Hence, the localized necking becomes very mesh dependent. In fracture mechanics, computational cells are used to introduce a physical length-scale into the finite element model over which continuum damage occurs. Computational cells are finite elements in the process zone having their characteristic size determined by the physical process under consideration [38]. A similar route may be taken to describe plastic failure in the steel pipeline when using shell elements, i.e. the characteristic element length is determined by the length scale of the phenomenon responsible for failure. Assume that the length scale of local necking, i.e. the width of the local neck, is about the sheet thickness. It is then reasonable to expect that a mesh with characteristic element size about equal to the sheet thickness would give good results. For the results presented in this paper, the initial minimum element size in the FE mesh used is approximately 4.3 mm. To ensure unit aspect ratio at failure, the elements along the predefined seam of failing elements have a length of 15 mm in the pipe axial direction. The remaining elements in the pipe have element edge sizes of approximately 15 mm.

Due to the symmetry of the full scale experiments (see Figure 5), only half of the total pipe length was modeled (see Figure 4). The FE-mesh of the short steel pipeline (Methane gas simulations) consists of 21774 Belytschko-Tsay shell elements with five through-thickness integration points. The long pipeline mesh (Hydrogen gas simulations), consists of 65493 elements. Referring to the coordinate system in Figure 4, constraints in y-direction on the bottom nodes of the pipe ensures no movement of the pipe. In addition to this, symmetry conditions are applied on the side of the pipe where the initial crack is generated. The crack is then driven by the internal pressure profile along a predefined crack path. As

illustrated in Figure 4, this crack path is modeled as a predefined "seam" where the elements are allowed to fail. Thus, the crack is restricted to propagation in the longitudinal direction of the pipeline.

5 Results

This section presents calculations performed with the coupled model and comparisons with experimental data. The same spatial resolution is always used for both the pipeline model and the fluid model in the axial direction. Though it is not shown in this paper, it is found that using a finer spatial resolution in the fluid code than in the structural code does not affect the results of the simulations. Furthermore, the Courant–Friedrichs–Lewy (CFL) number for the fluid part of the simulations was set to 0.9. This practically means that the time step is set such that the pressure waves advance of at most 0.9 cell length in each calculation step. The parameter values for the EOS (8) are summarized in Table 3. The same set of material parameters (Table 2) and meshes were used in all simulations.

Table 4 shows a comparison between the predicted and experimental fracture-propagation length (l_f), maximum and average speed of fracture (v_f). It is seen that the numerical predictions show a very good agreement with the full-scale experimental measurements. Furthermore, as demonstrated in Figure 6 , the experimental pressure measurements at 1 and 3(4) meter, as well as the crack position versus time, are very similar to the simulated results for all four cases.

One reason for the difference between the simulated and experimental crack position versus time curves close to crack arrest is that in the experiments, the crack turns away (meanders) from the axially propagating crack when it approaches arrest. From inspection of the pipelines after the experiments, this sometimes happens in the last 1-5 cm of the total crack path. We do not have an explanation for this experimental observation – nor can it be reproduced in the simulations. The distance between the

timing wires (20 cm in the methane tests and 10 cm in the hydrogen test) also limits the possibility to resolve the true fracture position close to crack arrest.

In Figure 7 a comparison of the simulated and experimentally obtained shape of the ruptured part of the pipeline is shown. Despite the excellent agreement between the experimental and simulated pressure readings and crack positions (Figure 6), it is observed that the simulated shape of the pipe attains a strongly exaggerated wavy shape when compared to the experimental case. In Figure 8 the RDF is pictured from the side after approximately 85 cm of propagation for both the experiment and the simulation of the 152 bar methane experiment. A high speed camera capturing images at 100 kfps was used in the full scale experiment. From the figure it is observed how the opening parts of the pipe differ in the experiment and the simulation. Whereas the picture from the experiment shows a relatively shallow rise of the opening parts – one can see how opening parts rises much "steeper" in the simulation.

6   Discussion

The fluid-structure interaction model presented in this paper can be used to predict the total propagation of a running ductile fracture in a high pressure pipeline. Despite a number of simplifications regarding the modelling of the fluid and the material behaviour, direct comparison with four full scale experiments shows that both the pressure evolution in front of the RDF and the crack position can be well predicted numerically. In the following a discussion related to two main challenges will be given.

6.1   Structural modelling challenges

Perhaps the most challenging issue in the modelling of ductile crack growth is that the simulation results often depend on the refinement of the FE mesh. Ideally in an FE simulation, the results should converge towards the actual solution of the boundary value problem (often being an analytical solution or

experimental result) when the size of the elements are decreased. As mentioned in Section 4.3; numerical simulation of plastic localization using shell elements can lead to mesh dependence. When using the default shell element in LS-DYNA (Belytschko-Tsay), regularization techniques are necessary to achieve convergence. However, by choosing an element size of the order of the thickness, relatively good results can be expected. Following the arguments in [29], we have chosen to use an initial element aspect ratio that gives a close to square element shape at the onset of fracture. Since the loading is primarily in the circumferential direction, the "seam" of elements that are allowed to fail are initially three times as long in the axial direction as in the hoop (reference) direction. Further refinement of the failing elements, e.g. by halving the elements sizes in the hoop direction to $1/5^{th}$ of the pipe thickness, makes the RDF propagate much further – leading to a fully ruptured pipeline. By keeping the same element size in the hoop direction, and only refining the axial length of the elements (giving a different aspect ratio at fracture), the RDF will not differ significantly from the results presented in this paper. In this work, the crack is restricted to propagation along a predefined "seam" in the longitudinal direction of the pipeline. Sensitivity of the direction of the crack propagation with respect to mesh alignment will be a topic for further studies. As an alternative to using shell elements in combination with regularization techniques such as non-local approaches [39], cohesive zone elements could also be used. Nielsen and Hutchinson [40] stated that the cohesive zone in a large scale finite element model should represent that part of the behaviour that the plate or shell elements cannot capture.

6.2   Fluid modelling challenges

The ideal gas assumption used in the fluid part of the simulations, models the properties of the gases in the full-scale experiments reasonably well. In some of the tests, the escaping gas was observed to ignite, and this phenomenon is not captured by the model. It can, however, be argued that this happens on the

outside of the pipe only where oxygen is present, so that the driving force of the crack, namely the pressure within the pipe, is not affected. On the other hand, when applying the model to more complicated gas mixtures, e.g. mixtures involving CO_2, an extension of the model to more sophisticated EOS should be considered.

For a pipe with a running fracture, the pressure, and therefore the load on the pipe walls, will vary circumferentially inside the pipe [7]. The present one-dimensional flow model inside the pipe does not intrinsically account for such variations, and this will be the topic of future investigations.

7 Conclusion

A coupled fluid-structure model for pipeline integrity simulations has been developed. A comparison of numerical predictions and experimental data obtained from full-scale testing of running fracture in steel pipelines pressurized with hydrogen and methane was performed. Very good agreement was obtained between calculated and measured crack lengths and pressure profiles.

This work is one step towards the objective of developing a coupled (fluid-structure) fracture-assessment model to enable safe and cost-effective design and operation of high-pressure gas pipelines by improving the fundamental understanding of the interaction between the material-mechanical and fluid-dynamical behaviour.

8 Acknowledgments

9 References

1. IEA/OECD. Energy technology perspectives 2008 – Scenarios and Strategies to 2050. ISBN 978-92-64-04142-4.

2. Maxey, W.A. Fracture initiation, propagation and arrest. Fifth Symposium on Line Pipe Research, American Gas Association, 1974, Houston.

3. Sugie, E., Matsuoka M. and Akiyama, T. A Study of Shear Crack Propagation in Gas-Pressurized Pipelines. Journal of Pressure Vessel Technology, 1982;104(4):338-343.

4. Leis, B.N., Zhu X-K., Forte T.P., and Clark E.B. (2005). Modeling running fracture in pipelines - past, present, and plausible future directions in 11th International conference on fracture. Turin, Italy.

5. Higuchi, R., Makino, H., Matsumara, M., Nagase, M. and Takeuchi, I. Development of a New Prediction Model of Fracture Propagation and Arrest in High Pressure Gas Transmission Pipeline. 8th International Welding Symposium. Kyoto, Japan, 2008.

6. O'Donoghue, P.E., Green, S.T., Kanninen, M.F. and Bowles, P.K. The development of a fluid/structure interaction model for flawed fluid containment boundaries with applications to gas transmission and distribution piping. Computers & Structures 1991; 38 (5-6):501-513

7. O'Donoghue, P.E., Kanninen, M.F., Leung, C.P, Demofonti, G. and Venzi, S. The development and validation of a dynamic fracture propagation model for gas transmission pipelines. International Journal of Pressure Vessels and Piping 1997; 70(1):11-25.

8. O'Donoghue, P.E. and Zhuang, Z. Design of mechanical crack arrestors. Fatigue and Fracture of Engineering Materials and Structures 1999; 22(1):59-66.

9. You, X.C., Zhuang, Z., Huo, C.Y., Zhuang, C.J. and Feng, Y.R. Crack arrest in rupturing steel gas pipelines. International Journal of Fracture, 2003;123(1-2):1-14.

10. Yang, X.B., Zhuang, Z., You, X.C., Feng, Y.R., Huo, C.Y. and Zhuang, C.J. Dynamic fracture study by an experiment/simulation method for rich gas transmission X80 steel pipelines. Engineering Fracture Mechanics, 2008;75(18):5018-5028.

11. Greenshields, C.J., Venizelos G.P., and Ivankovic A., A fluid-structure model for fast brittle fracture in plastic pipes. Journal of Fluids and Structures 2000;14(2):221-234.

12. Terenzi, A., Influence des propriétés du fluide réel dans la modélisation de l'onde de détente interférant avec la propagation de la fracture ductile. Oil & Gas Science and Technology - Rev. IFP, 2005. 60(4):711-719.

13. Mahgerefteh, H., Oke A., and Atti O., Modelling outflow following rupture in pipeline networks. Chemical Engineering Science, 2006. 61(6):1811-1818.

14. Cumber, P.S., Outflow from fractured pipelines transporting supercritical ethylene. Journal of Loss Prevention in the Process Industries 2007;20(1):26-37.

15. Zhou, J. and Adewumi M.A., Simulation of Transient Flow in Natural Gas Pipelines. Pipeline simulation interest group, 1995. 95.

16. Rabczuk T, Gracie R., Song J.H. and Belytschko T. Immersed particle method for fluid-structure interaction, International Journal for Numerical Methods in Engineering, 2010;81(1):48-71.

17. Hallquist, J.O. LS-DYNA Keyword User's Manual, Livermore Software Technology Corporation. 2007.

18. Berstad T., Dørum C., Jakobsen J. P., Kragset S., Li H., Lund H., Morin A., Munkejord S.T., Mølnvik M. J., Nordhagen H. O. and Østby E.. CO2 pipeline integrity: A new evaluation methodology. International Conference on Greenhouse Gas Technologies (GHGT-10), Amsterdam, 2010.

19. Aihara, S., Østby, E., Lange, H.I. Misawa, K., Imai, Y. and Thaulow, C. Burst tests for high-pressure hydrogen gas line pipes. 7th International Pipeline Conference, Calgary, Canada, 2008.

20. Besson, J., Luu, T.T., Tanguy, B. and Pineau, A. Anisotropic plastic and damage behavior of a high strength pipeline steel. Proceedings of the International Offshore and Polar Engineering Conference, 2009.

21. Tanguy, B., Luu, T.T, Perrin, G., Pineau, A. and J. Besson. Plastic and damage behaviour of a high strength X100 pipeline steel: Experiments and modelling. International Journal of Pressure Vessels and Piping 2008;85(5):322-335.

22. Cockcroft, M.G. and Latham, D.J. Ductility and the workability of metals. J. Inst. Metals 1968;96:33-39.

23. Børvik, T., Olovsson L., Dey, S., Langseth, M. Normal and oblique impact of small arms bullets on AA6082-T4 aluminium protective plates. International Journal of Impact Engineering 2011;38(7):577-589.

24. Albertini, C. and Montagnani, M. Wave propagation effects in dynamic loading. Nuclear Engineering and Design 1976;37(1):115-124.

25. Rosakis, A.J. and Ravichandran, G. Dynamic failure mechanics. International Journal of Solids and Structures 2000;37(1-2):331-348.

26. Besson, J. Continuum Models of Ductile Fracture: A Review. International Journal of Damage Mechanics 2009;19 (1):3-52.

27. Murtagian, G.R. and Ernst, H.A. Dynamic axial crack propagation in steel line pipes. Part II: Theoretical developments. Engineering Fracture Mechanics 2005;72(16):2535-2548.

28. Arabei, A., Pyshmintsev, I.Y., Shtremel, M.A, Glebov, A.G., Struin A.O. and Gervasev, A.M. Resistance of X80 steel to ductile-crack propagation in major gas lines. Steel in Translation 2009;39(9):719-724.

29. Besson, J., Steglich D., and Brocks, W. Modeling of plane strain ductile rupture. International Journal of Plasticity 2003;19(10): 1517-1541.

30. Titarev V.A. and Toro E.F. MUSTA schemes for multi-dimensional hyperbolic systems: analysis and improvements. Int. J. Numer. Meth. Fluids 2005;49:117–147.

31. Toro E.F. MUSTA: A multi-stage numerical flux. Appl. Numer. Math. 2006;56:1464–1479.

32. Munkejord S.T., Evje S. and Flåtten T. The multi-stage centred-scheme approach applied to a drift-flux two-phase flow model. Int. J. Numer. Meth. Fluids 2006;52:679–705.

33. Munkejord S.T., Jakobsen J.P., Austegard A. and Mølnvik M.J. Thermo- and fluid-dynamical modelling of two-phase multi-component carbon dioxide mixtures. Int. J. Greenh. Gas Con. 2010;4:589–596.

34. Munkejord S.T., Evje S. and Flåtten T. A MUSTA scheme for a nonconservative two-fluid model. SIAM J. Sci. Comp. 2009;31:2587–2622.

35. Dørum C., Lademo O.-G., Myhr O.R., Berstad T. and Hopperstad O.S. Finite element analysis of plastic failure in heat-affected zone of welded aluminium connections, Computers and Structures 2010;88:519-528.

36. Wang T., Hopperstad O.S., Lademo O-G. and Larsen P.K. Finite element analysis of welded beam-to-column joints in aluminium alloy EN AW 6082 T6. Finite Elements in Analysis and Design 2007;44:1–16.

37. Fyllingen Ø., Hopperstad O.S., Lademo O.-G. and Langseth M. Estimation of forming limit diagrams by the use of the finite element method and Monte Carlo simulation, Computers and Structures 2009;87:128-139.

38. Nègre P., Steglich D. and Brocks W. Crack extension at an interface. Prediction of fracture toughness and simulation of crack path deviation. International Journal of Fracture 2005;134:209–29.

39. Pijaudier-Cabot G. and Bazant Z.P. Nonlocal damage theory. Journal of Engineering Mechanics 1987;113:1512–1533.

40. Nielsen K.L and Hutchinsen J.W. Cohesive traction-separation laws for tearing of ductile metal plates. International Journal of Impact Engineering 2011, *in press*.
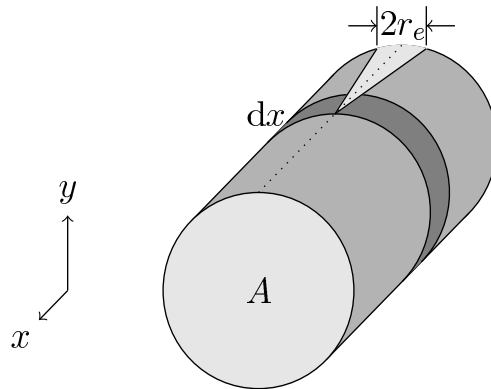
Figure 1. The crack propagates along the *x*-direction, leaving behind a growing opening of width $2r_e(x)$ in the pipe. As the crack symmetrically propagates in both directions, only half of the domain is shown.
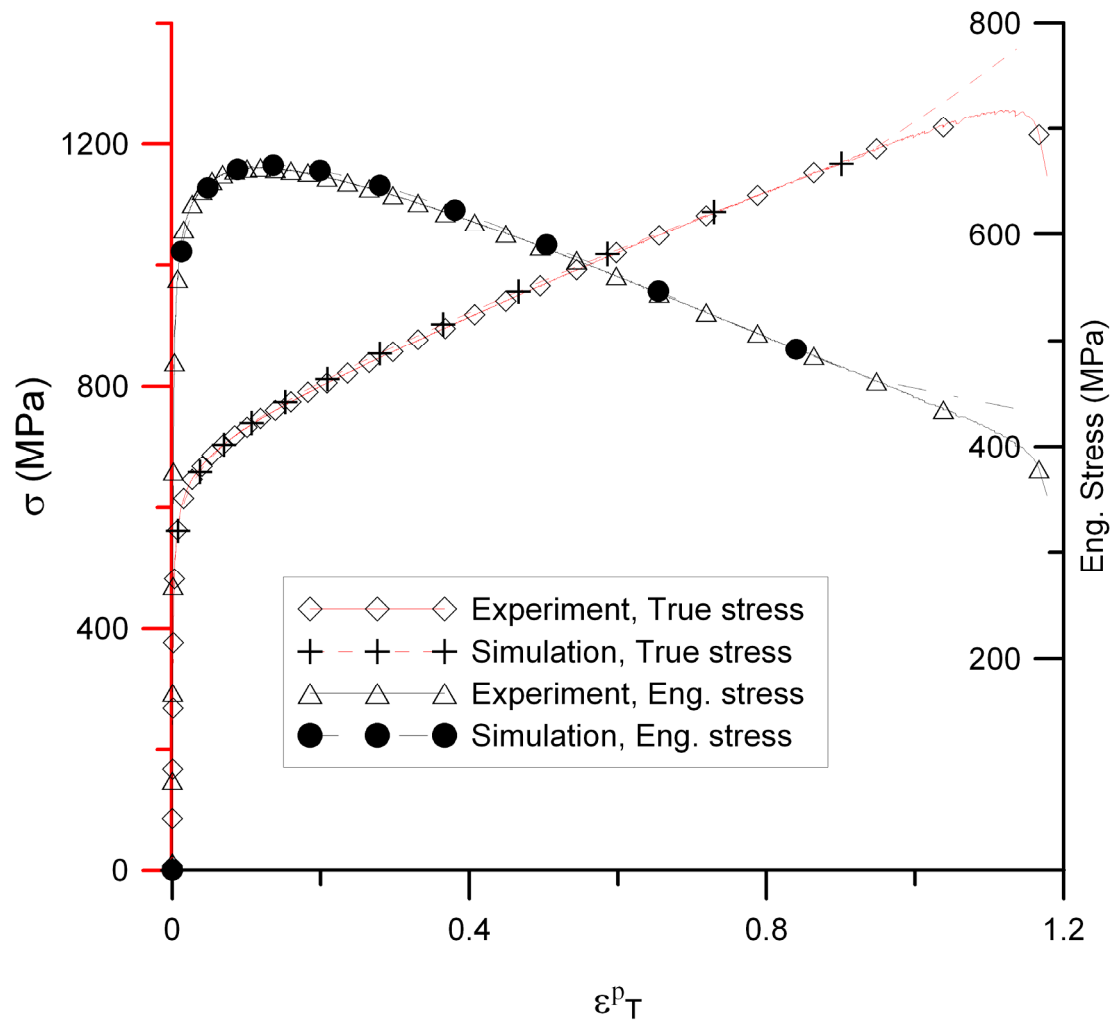
Figure 2. Quasi-static true and engineering stress vs. true plastic strain curves. Experimental curve shown with solid lines and simulation with calibrated material parameters shown in dashed lines.
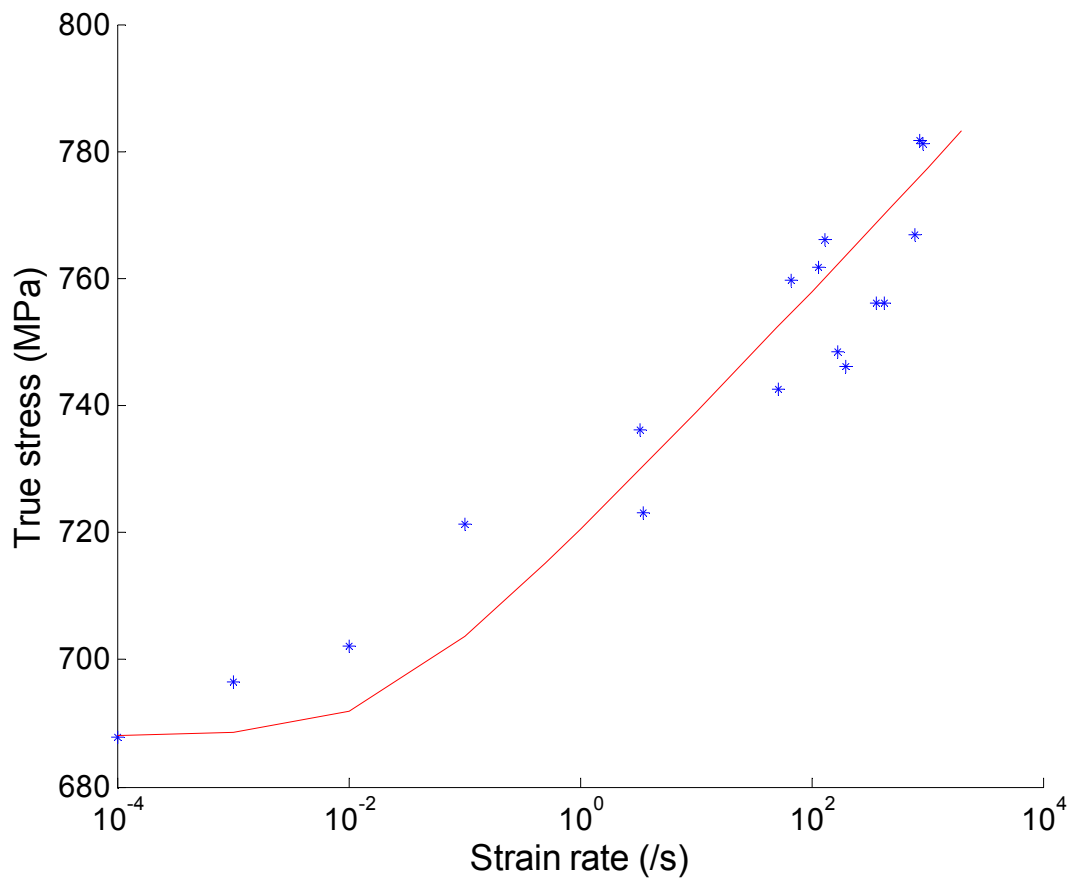
Figure 3. True stress at 2% plastic strain for experiments performed at different strain rates (marked as stars). The solid line represents the fitted strain rate sensitive hardening law (Eq. 2) using $\dot{\varepsilon}_0 = 1.5 \times 10^{-2}$ s^{-1} and $c = 1.1 \times 10^{-2}$
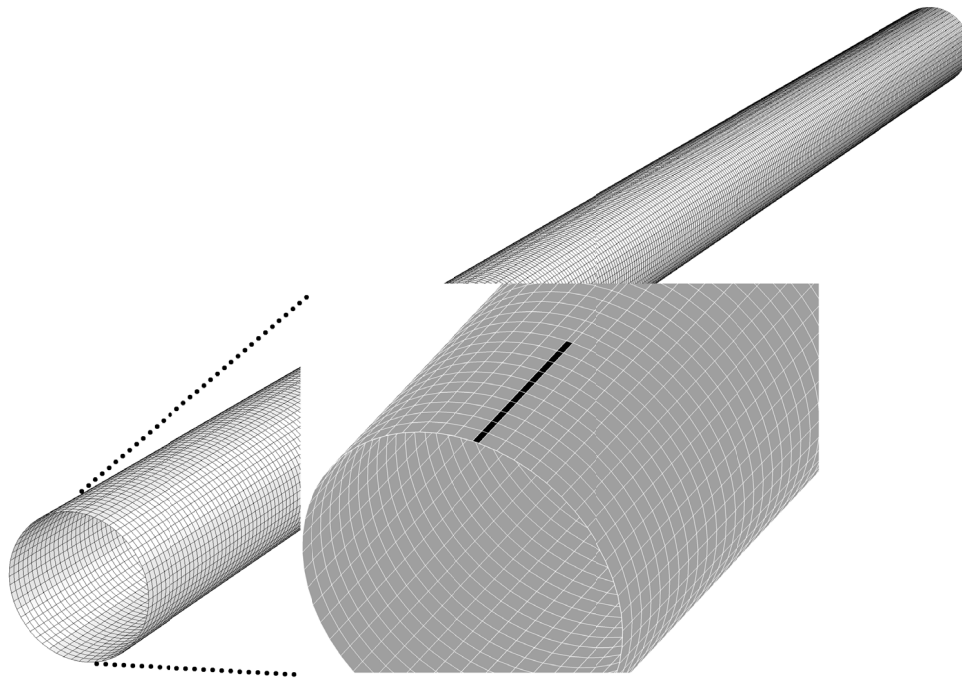
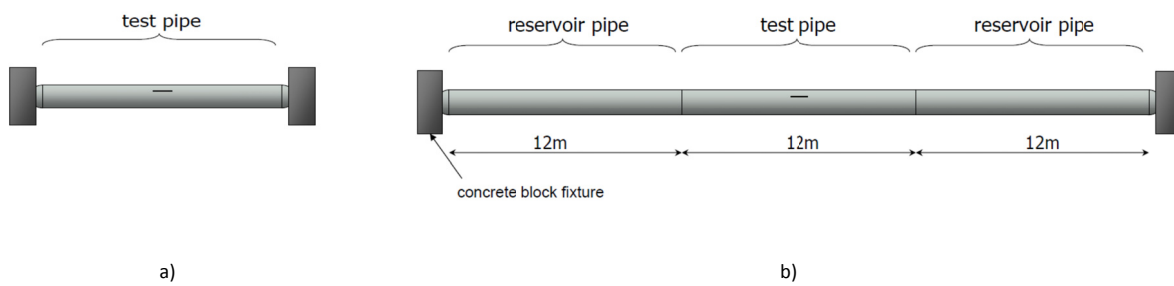Figure 4. The FE-mesh of the pipe in LS-DYNA (the elements representing the explosive charge are highlighted).

a)

b)

Figure 5. Schematic illustration of a) Methane gas test setup and (total 11.5 meter) b) Hydrogen gas test setup (total 34.5 meter).
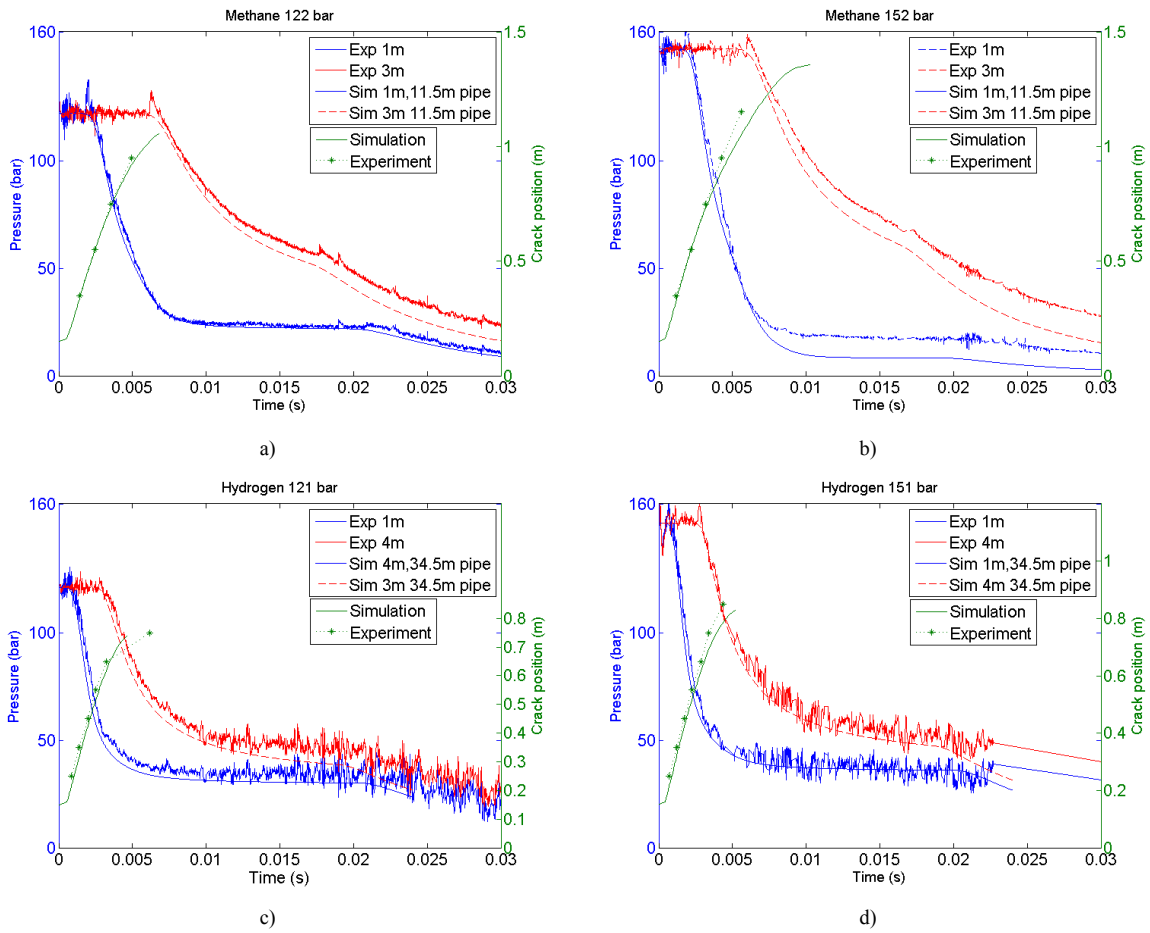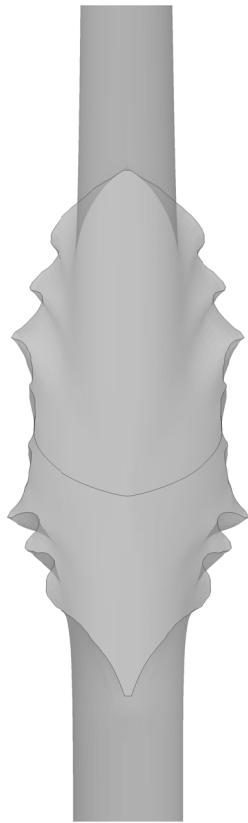
Figure 6. Comparison of predicted and measured pressure in pipeline, and the crack position history of the simulations and experiments, a-b) methane gas pressurized at 122 and 152 bar, and c-d) hydrogen gas pressurized at 121 and 151 bar.
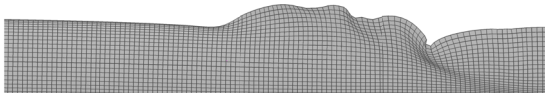
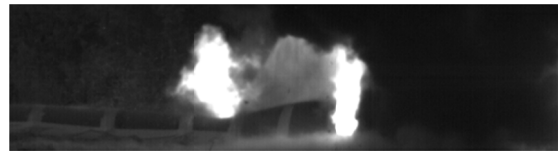a)   b)

Figure 7. Pictures of pipeline (Methane at 122 bar) after crack arrest. Simulated picture is seen in a) and picture after the full scale experiment seen in b).

a)   b)

Figure 8. Pictures of the simulated (a) and experimental RDF (b) for the 152 bar methane experiment. Crack position is approximately 1m from the middle of the pipe in both pictures. Notice the difference in the opening parts of the pipe right behind the crack tip.

Table 1. Chemical composition (wt%) of API 5L-X65mod. ERW steel (produced by Nippon steel).

C	Si	Mn	P	S	Nb	V
0.10	0.20	1.47	0.012	0.004	0.048	0.025

Table 2: Work-hardening parameters for API 5L-X65mod. ERW steel.

σ_0 (MPa)	Q_1 (MPa)	Q_2 (MPa)	C_1 (−)	C_2 (−)	S_{100} (MPa)	$\dot{\varepsilon}_0$ (s^{-1})	c (−)
486.2	126.9	227.6	122.8	7.537	980.0	0.015	0.011

Table 3. EOS parameter values used in the simulations.

	$\gamma = c_p/c_v$	c_p (J kg^{-1} K^{-1})
Hydrogen, 121 bar	1.5307	12784
Hydrogen, 151 bar	1.5596	12557
Methane, 122 bar	1.6153	1114.1
Methane, 152 bar	1.8059	933.72

Table 4. Comparison of predicted and experimental fracture propagation lengths.

	Simulated l_f (m)	Experimental l_f (m)	Simulated max v_f (m/s)	Experimental max v_f (m/s)
Hydrogen, 121 bar	0.59	0.60-0.70	199	200-205
Hydrogen, 151 bar	0.68	0.75-0.80	217	205-215
Methane, 122 bar	0.91	0.91	218	200-210
Methane, 152 bar	1.21	1.16	235	210-220